Published in final edited form as:
Neurobiol Dis. 2008 November ; 32(2): 309–318. doi:10.1016/j.nbd.2008.07.014.

Significant structural but not physiological changes in cortical neurons of 12-month-old Tg2576 mice

Anne B. Rocher, **Michael S. Kinson**, and **Jennifer I. Luebke***
Department of Anatomy and Neurobiology, M949, Boston University School of Medicine, 85 E. Newton St., Boston, MA 02118

Abstract

Amyloid-beta (Aβ) plays a key role in the etiology of Alzheimer's disease. Pyramidal cell dendrites exposed to Aβ exhibit dramatic structural alterations, including reduced dendritic spine densities. To determine whether such structural alterations lead to electrophysiological changes, whole-cell patch clamp recordings with biocytin filling were used to assess both the electrophysiological and morphological properties of layer 3 pyramidal cells in frontal cortical slices prepared from 12-month-old Tg2576 amyloid precursor protein (APP) mutant vs. wild-type (Wt) mice. Tg2576 cells exhibited significantly increased dendritic lengths and volumes and decreased spine densities, while the total number of spines was not different from Wt. Tg2576 and Wt cells did not differ with regard to passive membrane, action potential firing or glutamatergic spontaneous excitatory postsynaptic current properties. Thus, overexpression of mutated APP in young Tg2576 mice leads to significant changes in neuronal morphological properties which do not have readily apparent functional consequences.

Keywords

Amyloid-beta; Alzheimer's disease; dendritic spine; frontal; patch-clamp; slice; glutamatergic synaptic transmission

INTRODUCTION

Tg2576 transgenic mice overexpress the Swedish mutation of the human amyloid precursor protein (APP) gene and are a widely employed model of aberrant amyloid deposition in Alzheimer's disease (AD). Tg2576 mice exhibit progressive increases in soluble and fibrillar Aβ peptides and deposits in the brain, resulting in neuropathological alterations and behavioral deficits reminiscent of AD (Hsiao, 1998). In these mice, high levels of soluble Aβ species are present by 6 months of age and fibrillar plaque deposition first appears at about 11–12 months of age (Kawarabayashi et al., 2001; Lehman et al., 2003). Numerous studies have established that proximity to fibrillar Aβ plaques is associated with dystrophic dendrites and axons, aberrant sprouting and increased curvature of dendritic processes and dramatic reductions in dendritic spine density with accompanying synapse loss in hippocampal and neocortical pyramidal cells (Knowles et al., 1999; Urbanc et al., 2002; Tsai et al., 2004; Spires et al., 2005; Meyer- Luehmann et al., 2008; review: Spires and Hyman, 2004). Less is known about

*Correspondence to: Jennifer I. Luebke, PhD., M949, Boston University School of Medicine, 85, E. Newton St., Boston, MA 02118; e-mail: E-mail: jluebke@bu.edu, phone: 617 638-5995, fax: 617 638-5954.

the effect of endogenous soluble Aβ species on neuronal morphology in younger Tg2576 mice prior to substantial fibrillar plaque deposition, nor about the effects of Aβ on global dendritic morphology of entire cells.

It has long been hypothesized that Aβ-induced morphological changes in a given cell lead to functionally relevant alterations in electrophysiological properties, because morphology is a fundamental determinant of synaptic integration and neural firing patterns (Mainen and Sejnowski, 1996; Euler and Denk, 2001; Krichmar et al., 2002; Vetter et al., 2001). The dramatic reduction in density of dendritic spines (the principal postsynaptic substrate for glutamatergic inputs) might plausibly lead to significant reductions in excitatory synaptic responses. Indeed, a number of studies have shown that both exogenous and endogenous Aβ significantly reduce glutamatergic synaptic responses in the hippocampus (review: Walsh and Selkoe, 2004; Jacobsen et al, 2006; Venkitaramani et al., 2007; Parameshwaran et al., 2008). Interestingly, there is evidence that the effects of Aβ on glutamatergic synaptic signaling may be more prominent in the hippocampus than elsewhere in the brain. For example, *in vivo* studies have shown that glutamatergic synaptic transmission is unaltered in the neocortex of APP mutant mice at a young age (Roder et al., 2003; Stern et al., 2004), even while it is impaired in the hippocampus of the same subjects (Roder et al., 2003). While the previous identifications of structural changes are important, they cannot be used to make definitive conclusions about the functionality of a given cell in the absence of empirical evidence. The question of the relationship between structure and function of individual frontal cortical cells in Tg2576 versus Wt mice was therefore addressed for the first time in the present study.

MATERIALS AND METHODS

Experimental subjects

Two Tg2576 transgenic and two wild-type (Wt) mice (12 months old, female) were used in this study. Tg2576 mice bred on a C57B6/SJL background and overexpressing the Swedish mutation of human APP, and Wt mice were obtained from the Boston University Alzheimer Disease Center (ADC) transgenic mouse facility. Founders for the Tg2576 colony were kindly provided by Dr. Hsiao-Ashe (Hsiao et al., 1996; Hsiao, 1998). Mice were genotyped using a standardized PCR assay on tail DNA. Mice were housed under standard conditions with *ad libidum* access to food and water at the Boston University Laboratory Animal Science Center (LASC), a fully accredited International Association for Assessment and Accreditation of Laboratory Animal Care (AAALAC) facility. Animal care was maintained at standards directed by both the National Institutes of Health *Guide for the Care and Use of Laboratory Animals* and the U.S. *Public Health Service Policy on Humane Care and Use of Laboratory Animals* and approval for all procedures was obtained from the Boston University Institutional Animal Care and Use Committee (IACUC). While the number of 12-month-old subjects available for the present study was limited, the total number of neurons studied was not, as electrophysiological recordings were obtained from 19 Wt and 31 Tg2576 neurons, and of these, 8 Wt and 9 Tg2576 neurons were filled for extremely detailed morphometric analyses that yielded a total of 52,090 dendritic spines from Wt and 52,181 from Tg2576 mice. Moreover, while the within-group variability of all data was small, for a number of specific parameters the between-group differences were large (see Table 1), revealing significant differences between Wt and Tg2576 neurons.

Slice preparation

Mice were sacrificed by decapitation and their brains were immediately extracted and placed into ice-cold oxygenated (95% O_2, 5% CO_2) Ringer's solution (concentrations in mM): 26 $NaHCO_3$, 124 NaCl, 2 KCl, 3 KH_2PO_4, 10 Glucose, 2.5 $CaCl_2$, 1.3 $MgCl_2$ (pH = 7.4, Fluka, NY). The cortical hemispheres were dissected as a block and affixed with cyanoacrylate glue

to an agar slab secured in a tissue holder. Three hundred micron thick coronal slices of the rostral third of the brain were cut in ice-cold oxygenated Ringer's solution with a vibrating microtome and then placed in room-temperature oxygenated Ringer's solution for at least 1 hour prior to recording. Single slices were transferred to submersion-type recording chambers (Harvard Apparatus, Holliston, MA) on the stages of Nikon E600 infrared-differential interference contrast microscopes (IR-DIC, Micro Video Instruments, Avon, MA) for recording. Slices were continuously perfused with room-temperature, oxygenated Ringer's solution at a rate of 2–2.5 ml per minute.

Whole-cell patch clamp recordings

Studies focused on layer 3 pyramidal cells because of the key role these neurons play in the mediation of cognitive function (review: Morrison and Hof, 2002). Layer 3 pyramidal cells in frontal cortical slices were identified under IR-DIC optics. Previous experiments in this laboratory have determined that fibrillar plaques are readily identifiable under IR-DIC optics (unpublished observations). As described below, fibrillar plaques were scarce in slices from Tg2576 mice processed with thioflavin-S, and visible plaques were also rarely observed under IR-DIC optics in slices from Tg2576 mice from which recordings were obtained. Standard whole-cell patch clamp recordings (Edwards et al., 1989; Luebke et al., 2004; Chang et al., 2005; Chang and Luebke, 2007) were used to examine electrophysiological properties. Nonheparinized microhematocrit capillary tubes (Fisher, Pittsburgh, PA) were pulled into patch electrode pipettes on a Flaming and Brown horizontal micropipette puller (Model P87, Sutter Instruments, Novato, CA). The potassium gluconate (KGlu) internal solution used for recording had the following composition (concentrations, in mM): 122 KGlu, 2 $MgCl_2$, 5 EGTA, 10 NaHEPES, 2 MgATP, 0.3 NaGTP, and 1% biocytin (pH=7.4; Sigma, St. Louis, MO). With this internal solution, pipettes had resistances between 3 and 6 MΩ in the external solution. Data were acquired with either an EPC-9 or an EPC-10 amplifier (HEKA Elektronik, Lambrecht, Germany) controlled by "PatchMaster" acquisition software (HEKA Elektronik, Lambrecht, Germany) and recordings were low-pass filtered at 10 kHz.

Characterization of passive membrane properties

Passive membrane properties, including resting membrane potential (V_r), input resistance (R_n), and membrane time constant (τ), were assessed with current-clamp recordings from a membrane potential of −70 mV. V_r was measured as the voltage recorded when injected current was 0. For determination of R_n, the steady-state values of the voltage responses to a series of 200 ms current steps from −120 to +20 pA (8 steps, 20 pA per step) were plotted as a voltage-current relationship. R_n was calculated as the slope of the best-fit line through these data points. τ was calculated by fitting a single-exponential function to the first 100 ms of a 40 pA hyperpolarizing 200 ms current step.

Characterization of single action potential (AP) and repetitive AP firing properties

Single AP properties measured were: threshold, amplitude and rise time. The first AP produced by the 200 ms current-clamp series was used for single AP measurements. The threshold for firing was measured by expanding the time scale of the digitized trace and measuring the voltage at the point in the trace when the steep upward deflection of the spike began, and AP amplitude was measured from threshold to the peak of the spike. Repetitive AP firing was elicited by a series of 2 s current pulses (9 steps, −20 to +380 pA, 50 pA per step). APs were counted using "FitMaster" software (HEKA Elektronik, Lambrecht, Germany) event detection and then plotted against current step, yielding a frequency-current plot.

Characterization of spontaneous excitatory postsynaptic current (sEPSC) properties

Baseline sEPSC data were acquired under voltage-clamp at a holding potential of −80 mV for a period of 2 min. sEPSC data were subsequently analyzed using the MiniAnalysis program (Synaptosoft, Decatur, GA). Events were required to exceed a detection threshold set at the maximum of the RMS noise level (5 pA) and to have a rise time greater than 0.5 ms. For each cell, the following characteristics of sEPSCs were determined: frequency, amplitude, rise time constant and decay time constant (Luebke and Rosene, 2003; Luebke et al., 2004). The rise time constant and the decay time constant were determined by fitting averaged traces (a minimum of 100 events per cell) to a single exponential function in each case.

Processing and confocal scanning of biocytin-filled streptavidin-Alexa 488 labeled cells

Following recordings (during which cells were simultaneously filled with biocytin), slices were transferred to a solution of 4% paraformaldehyde in 0.1 M phosphate buffered saline (PBS), pH 7.4, and stored at 4°C overnight. The following day, slices were successively incubated in: PBS, 3 rinses of 10 min each; 0.1% Triton X-100 in PBS for 2 h at room temperature; and streptavidin-Alexa 488 (1:500, Vector Labs, Burlingame, CA) at 4°C for 48 h. In addition, slices caudal to the frontal cortex (and thus not used for recordings) from Tg2576 mice were incubated in a 0.01% thioflavin-S (Sigma, St. Louis, MO) solution for 20 min to visualize fibrillar Aβ deposits. Following processing, slices were mounted in Prolong Gold (InVitrogen, Eugene, OR) and coverslipped. The fluorescence emitted by Alexa-488 under Argon laser excitation was detected with a Zeiss 510 confocal laser scanning microscope equipped with a Plan-Apochromat 40x/1.3 NA, 210 μm working-distance oil objective and a 505 nm long pass filter. Approximately 10 stacks (each with a 153 μm^2 field of view) per cell were captured with a digital zoom of 1.5x. Each stack was acquired at very high resolution, with an image size of 1536 × 1536 pixels, and a voxel size of 0.1 × 0.1 × 0.2 μm for the x, y and z axes respectively.

Data processing and three-dimensional (3D) morphologic analyses

Pre-processing of image stacks—Each image stack was deconvolved (AutoDeblur, Media Cybernetics, Bethesda, MD) to reduce signal blurring. Deconvolved stacks were aligned in 3D and then integrated into a single volumetric dataset using Volume Integration and Alignment System (VIAS) software (Rodriguez et al., 2003; available at: http://www.mssm.edu/cnic). The integrated file was initially analyzed with the VIAS measure tool to record the distance of the soma from the pial surface, and the horizontal and vertical extents of the apical and basal dendritic trees.

Morphometric analyses of somata and dendrites—For analyses of somatic and dendritic parameters with AutoNeuron software (MBF Bioscience, Williston, VT), it was necessary to subsample the very large VIAS files (~15 GB in size), as this software is limited to data files no greater than 1 GB in size. The single volumetric data set obtained from VIAS was subsampled using TIFF Stack Subsampler (TSS) software (available at: http://www.mssm.edu/cnic), reducing by 75% the number of voxels, while accurately preserving dendritic morphology. In order to produce accurate subsampled stacks, TSS uses a 3D fractional binning approach to weigh the contribution of individual voxels to voxels in the new dataset while allowing subsampling to an arbitrarily smaller size. This method preserves the appearance of small features and gradients in the data and is also effective in improving the signal to noise ratio of the image. The subsampled data were imported into AutoNeuron for automatic 3D reconstruction of cells which were then exported to the companion NeuroExplorer software (MBF Bioscience, Williston, VT) for detailed morphometrics. The morphological parameters quantified by NeuroExplorer included: 1) soma volume; 2) total dendritic length and volume; 3) mean diameter for each dendritic segment; 4) dendritic length and branch point (node) distribution, as determined by Sholl analysis (regularly spaced, 25 μm

radius, concentric spheres centered on the soma were used, and dendritic length and number of nodes determined for each radius progressively distal from the soma), and; 5) dendritic curvature ratios (end-to-end linear distance of a dendritic segment/total length between the two segment ends) were calculated for each dendritic segment in either the apical or basal tree, and then a "mean curvature ratio" for a given tree was estimated by averaging the curvature ratios for all dendritic segments in that tree.

Spine detection and analyses—Dendritic spines were detected using the 64-bit version of NeuronStudio (Wearne et al., 2005; available at: http://www.mssm.edu/cnic) on the full-resolution stacks produced by VIAS integration. Subsampling of the data was not required since NeuronStudio is capable of working with very large data files (>20 GB). Using NeuronStudio the entire dendritic structure of each cell was automatically traced and subsequently dendritic spines were detected automatically by the program around the traced dendrites using a Rayburst-based spine analysis routine (Rodriguez et al., 2003; Rodriguez et al., 2006; Radley et al., 2008). Spine detection was performed on dendritic trees as a whole and on processes within concentric 50 μm circles at increasing distance from the soma (Sholl analysis). An operator then inspected each cell and made minor corrections as needed using the NeuronStudio interface.

Cell inclusion criteria

Electrophysiology—Only cells that met the following criteria were included in the electrophysiology data pool: a resting membrane potential of ≤ −55 mV (or a holding current of < 100 pA at −70 mV), stable access resistance, the presence of an AP overshoot and the ability to fire repeatedly during sustained depolarizing steps. There was no difference in the percentage of cells that met these criteria in the two groups of mice (>90% in each case).

Morphology—Only cells that met electrophysiological criteria were included in morphological analyses. In addition, all cells included in the morphological analyses were required to have an intact soma and a completely filled dendritic tree, with the apical tuft reaching the pial surface.

Statistical analyses

Following initial analyses, electrophysiological and morphological data were exported to Microsoft Excel and Prism 4 (GraphPad, San Diego, CA) databases for complete statistical analyses. For most analyses, the two-tailed Student's t-test was used to compare data from Wt vs. Tg2576 cells. The Kolmogorov-Smirnov non-parametric test was used to compare the cumulative percentiles of sEPSC inter-event intervals (frequencies) and amplitudes, and curvature ratios of dendritic segments in the Tg2576 vs. Wt groups. Sholl analysis data were compared by two-way ANOVA with genotype as the between-group factor and distance from the soma as the within-group factor. Bonferroni's test was then used in post hoc analyses. For correlation analyses, linear regression and Pearson's Product Moment correlations were used both to compute R_n from current-voltage plots and to determine the relationship between electrophysiological and morphological data in individual cells. The null hypothesis for each test was rejected at a threshold of 0.05. All data are presented as mean ± SEM.

RESULTS

A total of 19 visually identified layer 3 pyramidal cells in *in vitro* frontal cortical slices from the Wt mice and 31 cells from the Tg2576 mice met criteria for electrophysiological data analyses. Of these cells, 8 Wt and 9 Tg2576 cells met stringent criteria for further morphometric analyses. There was no difference in the electrophysiological response properties of morphologically characterized versus non-morphologically characterized cells within either

the Wt or Tg2576 groups; therefore, data from morphologically characterized and non-morphologically characterized cells were pooled for the overall electrophysiological analyses presented in the first part of the results section. Thioflavin-S staining of slices from the Tg2576 mice demonstrated that the number of fibrillar Aβ deposits was relatively low, as expected in these mice at this age (when soluble Aβ is the principal species present, Kawarabayashi et al., 2001; Lehman et al., 2003). A representative thioflavin-S stained slice and representative biocytin-filled pyramidal cells are shown in Fig. 1.

Passive membrane and repetitive AP firing properties were unaltered in cells from Tg2576 mice

Passive membrane properties of cells from Tg2576 mice did not differ significantly from cells from Wt mice (Fig. 2). Thus, the mean V_r was −63.7 ± 1.2 mV in Wt vs. −61.6 ± 1.2 mV in Tg2576, the mean τ was 17.0 ± 1.9 ms in Wt vs. 16.9 ± 1.7 ms in Tg2576, and the mean R_n was 127.7 ± 9.0 MΩ in Wt vs. 134.5 ± 9.2 MΩ in Tg2576. The mean threshold, rise time and amplitude of single APs did not differ in Tg2576 vs. Wt cells (threshold: −37.7 ± 1.2 mV for Wt, −39.7 ± 0.5 mV for Tg2576; rise time: 1.03 ± 0.04 ms for Wt, 1.01 ± 0.04 mV for Tg2576; amplitude: 85.5 ± 2.1 mV for Wt, 89.0 ± 1.2 mV for Tg2576). All cells displayed slowly adapting, regular spiking AP firing characteristics in response to a series of 2 s depolarizing current steps, exemplified by the representative cells in Fig. 2D. AP firing frequencies elicited by increasing depolarizing current steps were not significantly different in cells from Tg2576 mice compared to cells from Wt mice at any current step (Fig. 2E).

sEPSC properties were unaltered in cells from Tg2576 mice

Glutamate receptor-mediated sEPSCs recorded at a holding potential of −80 mV were mediated primarily by non-NMDA glutamate receptor activation as they were blocked by application of the non-NMDA glutamate receptor antagonist CNQX but not by the application of the NMDA receptor antagonist APV, and were unaltered in the presence of the $GABA_A$ receptor antagonist bicuculline methiodide (BMI) (not shown). Traces of sEPSCs in representative Wt and Tg2576 cells are shown in Fig. 3A. Neither the mean frequency nor the mean amplitude of sEPSCs were significantly different in the two cell groups (mean frequency: 1.9 ± 0.3 Hz in Wt and 2.5 ± 0.3 Hz in Tg2576; mean amplitude: 18.2 ± 0.2 pA in Wt and 20.8 ± 1.1 pA in Tg2576; Fig. 3B). Similarly, there were no significant differences in sEPSC kinetics between Tg2576 and Wt cells (rise time: 2.0 ± 0.4 ms in Wt and 1.5 ± 0.1 ms in Tg2576 and decay time: 11.6 ± 1.3 ms in Wt and 10.7 ± 1.7 ms in Tg2576; Fig. 3C).

General properties of morphologically characterized cells

Eight Wt and 9 Tg2576 electrophysiologically characterized cells met stringent criteria for detailed morphometric analyses using high-resolution confocal laser scanning microscopy. Examples of reconstructed pyramidal cells and of dendritic spines are shown in Fig. 4. The mean distance of somata from the pial surface did not differ between the Wt and Tg2576 cells (297 ± 27 μm for Wt; 347 ± 29 μm for Tg2576). The volume of somata was also similar in the two groups, at 796 ± 104 μm^3 for Wt and 955 ± 109 μm^3 for Tg2576 cells.

Dendritic length and volume were increased while branching complexity was unaltered in cells from Tg2576 mice

The mean vertical extents of the apical and basal dendritic trees did not differ between the Wt and Tg2576 cells, however the mean horizontal extents of both the apical and basal dendritic trees were significantly greater in Tg2576 than in Wt cells (Fig. 5A; Table 1; apical $p < 0.01$; basal $p < 0.04$). As shown in Fig. 5B and Table 1, the mean total volumes of both the apical and basal trees were also significantly greater in Tg2576 than the Wt cells (apical $p < 0.03$; basal $p < 0.002$), as were their mean total lengths (apical $p < 0.03$; basal $p < 0.02$). The mean

diameter of apical dendritic branches did not differ between groups, however the mean basal dendritic branch diameter was significantly greater in the Tg2576 compared to Wt cells (Fig. 5B; Table 1; $p < 0.02$). Sholl analysis of the number of branch points (nodes) in each of 10 (apical) or 4 (basal) concentric spheres at increasing (by 25 μm) radii from the soma was performed to determine whether Tg2576 cells exhibit increased branching complexity, which might, in part, account for the observed increase in dendritic volume (Fig. 5C). However, there was no difference in the branching complexity of either the apical or the basal trees in the two groups (Fig. 5C). Finally, the curvature ratios of dendritic branches demonstrated that the mean tortuosity of dendritic branches was not different for either apical or basal trees in Tg2576 vs. Wt cells (Table 1, Fig. 5D).

Dendritic spine number was preserved while spine density was decreased in cells from Tg2576 mice

Reconstructed apical and basal dendrites with spines from representative Tg2576 and Wt cells are shown in Fig 6A. Using high resolution confocal microscopy and automated spine detection in 3D, over 104,000 spines were counted on the 17 neurons included in the present study. The distribution and mean total number of dendritic spines in neither apical nor basal trees differed significantly in Tg2576 compared to Wt cells (Table 1; Fig. 6B). However, as shown in Fig. 6C, the mean density of spines per unit dendritic volume was significantly decreased in Tg2576 compared to Wt cells in both the apical and the basal trees ($p < 0.02$ for apical and $p < 0.01$ for basal spine density, Fig. 6C). Unlike with spine number, Sholl analysis revealed that spine density per micron was decreased in both the basal and apical trees consistently along the dendritic tree.

Mean total cell volume was significantly increased in cells from Tg2576 mice

The mean values for combined volumes of the somata plus dendrites were significantly different in the two groups, with Wt cells having a mean volume of $5581 \pm 353\ \mu m^3$ and Tg2576 cells having a mean volume of $8616 \pm 658\ \mu m^3$ ($p < 0.001$). Finally, the contribution of dendritic spines was included to estimate the total cell volume. While we did not measure spine volumes in the present study, Radley and coworkers (2008) have reported a mean spine volume of approximately $0.093\ \mu m^3$ in layer 3 frontal cortical pyramidal cells of the rat. This mean value, multiplied by the total number of spines for a given neuron was used to estimate the approximate total volume of spines for that neuron. Thus, the “total cell volume” was comprised of the sum of: soma volume, dendritic volume and estimated spine volume. The calculated total cell volume was greater in the Tg2576 cells, at $9216 \pm 693\ \mu m^3$ compared to $6118 \pm 413\ \mu m^3$ for Wt cells ($p < 0.002$).

As noted earlier, there were no significant differences in the electrophysiological data obtainedfrom morphologically characterized vs. non-morphologically characterized pyramidal cells ineither the Tg2576 or the Wt groups. Thus, in the morphologically characterized cells, there were no significant differences in passive membrane, AP firing or sEPSC properties between the Wt and Tg2576 groups. In light of the finding of a significantly reduced density of spines in theTg2576 compared to the Wt cells, similar to those reported by others for cortical pyramidal cells(review: Spires and Hyman, 2004), the preserved synaptic signaling is particularly interesting.Preserved glutamatergic signaling in the face of reduced dendritic spine density could plausiblybe due to the fact that, for any given cell, the total number of spines was preserved even while spine density per unit volume was significantly decreased. The most likely explanation forreduced density but not number of dendritic spines is the finding that the mean dendritic lengthsand volumes were significantly increased in Tg2576 cells. As shown in Fig. 6D, when total spine number were plotted against total cell volume for individual cells, a positive correlation wasobtained ($p < 0.02$), however when mean spine density was plotted against total cell volume there was no correlation. This indicates that the unchanged total

number of spines in the face of decreased density was likely due to the increased total cell volume in the Tg2576 cells.

DISCUSSION

It is widely accepted that abnormal Aβ processing and deposition play a key role in the etiology of Alzheimer's disease (AD). Hence, it is critically important to understand the toxic effect of soluble and fibrillar Aβ species on neurons; in this effort the use of APP mutant mice such as the Tg2576 strain is invaluable. The present study used *in vitro* slices prepared from the frontal cortex of Tg2576 mice at 12 months of age, when soluble but not fibrillar Aβ species are very abundant (Kawarabayashi et al., 2001; Lehman et al., 2003; Lesné et al., 2006), to address three important questions. First, are the basic electrophysiological or glutamatergic synaptic response properties of neurons in these mice altered? Second, is neuronal morphology altered and, if so, are structural changes spatially limited to individual processes or do they occur on a global level in a given cell? Third, are structural alterations associated with functional changes in individual neurons? The principal findings were that cells from Tg2576 mice exhibit: 1) no change in basic electrophysiological properties; 2) no change in glutamatergic sEPSC properties; 3) significantly increased dendritic lengths and volumes across the entire arbor, and; 4) no change in total dendritic spine number but a significant reduction in spine density along the entire dendritic arbor. In summary, Tg2576 cells exhibit significant structural changes in the absence of measurable electrophysiological changes.

The passive membrane and excitability properties of Tg2576 cells were unchanged. This finding of preserved basic electrophysiological properties is in agreement with *in vivo* evidence for unaltered resting membrane potential and AP firing rate of cortical neurons in 8–10 month old Tg2576 mice (Stern et al., 2004), and *in vitro* evidence that exogenous application of Aβ oligomers on cultured hippocampal neurons has no effect on their input resistance or AP discharge properties (Stern et al., 2004; Nimmrich et al., 2008).

The frequency, amplitude and kinetics of glutamatergic sEPSCs mediated by non-NMDA receptors also did not differ between Tg2576 and Wt cells. The finding of preserved glutamatergic signaling agrees with a report by Roder et al. (2003) of unaltered evoked glutamatergic synaptic responses in the frontal cortex (but reduced responses in the hippocampus) of APP23 transgenic mice, as assessed with field potential recordings both *in vivo* and *in vitro*. It is also consistent with a report by Stern et al. (2004) that evoked transcallosal synaptic potentials recorded in the neocortex *in vivo* are unaltered in 8–10 month old Tg2576 mice (whereas there is a 2.5-fold greater rate of synaptic response failure in >14 month old mice).

The intact glutamatergic signaling in the neocortex of APP mutant mice is interesting in light of the abundant published evidence that basal glutamatergic synaptic transmission is significantly reduced in the hippocampus of APP transgenic mice (review: Venkitaramani et al., 2007; Parameshwaran et al., 2008). *In vitro* field potential studies in hippocampal slices prepared from APP mutant mice (Hsia et al., 1999; Larson et al., 1999; Fitzjohn et al., 2001; Roder et al., 2003; Jacobsen et al., 2006; Saganich et al., 2006) and *in vivo* field potential studies (Giacchino et al., 2000) have demonstrated that glutamatergic synaptic signaling is significantly reduced in these mice even at a young age, when soluble Aβ species are abundant but fibrillar plaques have not yet been deposited. Aβ has also been shown to depress glutamatergic transmission as assessed by whole-cell patch clamp recordings of sEPSCs in cultured hippocampal neurons (Kamenetz et al., 2003; Hsieh et al., 2006; Nimmrich et al., 2008). The mechanism by which Aβ reduces glutamatergic transmission in the hippocampus is not completely understood, although there is evidence for AMPA receptor removal (Almeida et al., 2005; Hsieh et al., 2006), a decrease in the expression of NMDA receptors (Snyder et

al., 2005; Lacor et al., 2007), and for inhibition of presynaptic calcium channels at glutamatergic terminals (Nimmrich et al., 2008). The difference in findings in the neocortex versus hippocampus could be due to a number of factors, including: lower concentrations of Aβ in the cortex than in the hippocampus (as reported by Lehman et al., 2003), compensatory mechanisms present in the cortex but not hippocampus, consistent with behavioral studies showing preserved frontal cortical but impaired hippocampal function in Tg2576 mice, (King and Arendash, 2002; Middei et al., 2004), or lower vulnerability to the toxic effects of Aβ in the cortex compared to the hippocampus. Consistent with the idea that different cell types are differentially vulnerable to Aβ is the recent demonstration that layer 5 neocortical pyramidal cells are more resistant to the toxic effects of Aβ than are layer 3 cortical cells (Romito-DiGiacomo et al., 2007).

This is the first study to use high-resolution confocal microscopy and highly accurate 3D analyses to examine the detailed morphology, including total spine number and distribution, of APP mutant mouse neurons in their entirety. The properties of dendrites of Tg2576 cells were markedly different from Wt, with significant increases in spatial extents and dendritic lengths and volumes that extended across the entire apical and basal arbors. This finding is consistent with the report that increased $A\beta_{42}$ levels in neurites of cultured Tg2576 cells are associated with extensive sprouting of these neurites (Takahashi et al., 2004). By contrast, Alpar and coworkers (2006) report a decrease in dendritic length (but no change in volume) of apical dendritic branches of neocortical neurons in 11 month old Tg2576 mice. This discrepancy in findings may be due to differences in experimental and analytical approaches employed in the two studies; in particular, it is unclear whether the distance of the soma from the pial surface -a critical determinant of apical dendritic length- was similar in the Tg2576 and Wt groups in Alpar et al. (2006).

The present finding of increased dendritic lengths in Tg2576 neurons is interesting in light of many reports of increased dendritic sprouting, arborization and field size in the AD brain (for review: Spires and Hyman, 2004). The mechanism(s) of increased sprouting and elongation of dendrites is not yet known, although a number of factors could plausibly underlie these changes. First, dendritic elongation may be related to increased levels of neurotrophic factor in the vicinity of Aβ deposits in APP transgenic mice (Burbach et al., 2004). Second, the overexpression of APP *per se* could lead to dendritic elongation; indeed APP has been shown to exert trophic effects on dendrites *in vitro* (Qiu et al., 1995), possibly through inhibition of reelin which inhibits neurite outgrowth in cultured hippocampal neurons (Chin et al., 2007; Hoareau et al., 2008). Third, Aβ significantly alters intracellular calcium levels (Kawahara and Kuroda , 2000; Lacor et al., 2007), which play an important role in neurite outgrowth and regression in neurons (review: Mattson, 2007).

Importantly, a significant 26% reduction in spine density was observed in Tg2576 pyramidal cells, which is similar to the reduction in density reported by others (Spires et al., 2005; Alpar et al., 2006). This is the first demonstration that spine density decreases occur across entire apical and basal arbors of individual neurons in Tg2576 mice. However, while the mean density of spines was reduced across the entire dendritic arbor in Tg2576 cells, the total number of spines per neuron did not differ between Tg2576 and Wt cells. This finding emphasizes the importance of assessing both spine number and spine density across the entire dendritic extent. Given that there was a strong relationship between spine number (but not density) and total cell volume in individual cells, it appears that the total number of spines is maintained due to dendritic elongation in Tg2576 cells. The observed reduction in dendritic spine density in cells from 12-month-old Tg2576 mice is consistent with the idea that soluble forms of Aβ are toxic to dendritic spines. Soluble Aβ oligomers accumulate at synapses on dendritic spines (Lacor et al, 2004; Shankar et al., 2007) and have been demonstrated, *in vitro*, to cause spine regression by reducing the expression NMDA receptors (Snyder et al, 2005; Lacor et al. 2007) and by

reducing calcium influx through the NMDA receptors present on spines (Shankar et al, 2007). At this early stage of pathological progression, when few plaques are present but soluble Aβ species are abundant, there appears to be a compensatory dendritic elongation that occurs, resulting in the preservation of the total number of dendritic spines. After this age, fibrillar plaques develop rapidly and are associated with changes in neurite curvature and further dramatic decreases in spine density (Meyer-Luehmann et al., 2008). It is at this stage that the Aβ load is sufficient to cause progressive structural alterations to neurons, which likely have significant functional consequences, such as the abnormalities in cortical synaptic integration seen in fibrillar plaque-bearing mice *in vivo* (Stern et al., 2004). Further studies are needed to determine whether structural alterations in individual cells from older Tg2576 mice (in which plaques are more abundant) lead to functionally relevant changes in the electrophysiological behavior of the cells.

Acknowledgements

We thank Drs. Tara Spires, Carter Cornwall, Jason Radley and Doug Rosene for helpful comments on the manuscript, and Drs. Susan Wearne and Patrick Hof for helpful comments and technical advice on spine analyses. We also thank Joseph Amatrudo and Margaret Todd-Brown for technical assistance. Supported by NIA grant awards P30 AG13846 and R01 AG025062.

References

Almeida CG, Tampellini D, Takahashi RH, Greengard P, Lin MT, Snyder EM, Gouras GK. Beta-amyloid accumulation in APP mutant neurons reduces PSD-95 and GluR1 in synapses. Neurobiol Dis 2005;20:187–198. [PubMed: 16242627]

Alpar A, Ueberham U, Bruckner MK, Seeger G, Arendt T, Gartner U. Different dendrite and dendritic spine alterations in basal and apical arbors in mutant human amyloid precursor protein transgenic mice. Brain Res 2006;1099:189–198. [PubMed: 16781686]

Burbach GJ, Hellweg R, Haas CA, Del Turco D, Deicke U, Abramowski D, Jucker M, Staufenbiel M, Deller T. Induction of brain-derived neurotrophic factor in plaque-associated glial cells of aged APP23 transgenic mice. J Neurosci 2004;24:2421–2430. [PubMed: 15014117]

Chang YM, Luebke JI. Electrophysiological diversity of layer 5 pyramidal cells in the prefrontal cortex of the rhesus monkey: in vitro slice studies. J Neurophysiol 2007;98:2622–2632. [PubMed: 17804579]

Chang YM, Rosene DL, Killiany RJ, Mangiamele LA, Luebke JI. Increased action potential firing rates of layer 2/3 pyramidal cells in the prefrontal cortex are significantly related to cognitive performance in aged monkeys. Cereb Cortex 2005;15:409–418. [PubMed: 15749985]

Chin J, Massaro CM, Palop JJ, Thwin MT, Yu GQ, Bien-Ly N, Bender A, Mucke L. Reelin depletion in the entorhinal cortex of human amyloid precursor protein transgenic mice and humans with Alzheimer's disease. J Neurosci 2007;27:2727–2733. [PubMed: 17360894]

Edwards FA, Konnerth A, Sakmann B, Takahashi T. A thin slice preparation for patch clamp recordings from neurones of the mammalian central nervous system. Pflugers Arch 1989;414:600–612. [PubMed: 2780225]

Euler T, Denk W. Dendritic processing. Curr Opin Neurobiol 2001;11:415–422. [PubMed: 11502386]

Fitzjohn SM, Morton RA, Kuenzi F, Rosahl TW, Shearman M, Lewis H, Smith D, Reynolds DS, Davies CH, Collingridge GL, Seabrook GR. Age-related impairment of synaptic transmission but normal long-term potentiation in transgenic mice that overexpress the human APP695SWE mutant form of amyloid precursor protein. J Neurosci 2001;21:4691–4698. [PubMed: 11425896]

Giacchino J, Criado JR, Games D, Henriksen S. In vivo synaptic transmission in young and aged amyloid precursor protein transgenic mice. Brain Res 2000;876:185–190. [PubMed: 10973607]

Hoareau C, Borrell V, Soriano E, Krebs MO, Prochiantz A, Allinquant B. Amyloid precursor protein cytoplasmic domain antagonizes reelin neurite outgrowth inhibition of hippocampal neurons. Neurobiol Aging 2008;29:542–553. [PubMed: 17169463]

Hsia AY, Masliah E, McConlogue L, Yu GQ, Tatsuno G, Hu K, Kholodenko D, Malenka RC, Nicoll RA, Mucke L. Plaque-independent disruption of neural circuits in Alzheimer's disease mouse models. Proc Natl Acad Sci U S A 1999;96:3228–3233. [PubMed: 10077666]

Hsiao K. Transgenic mice expressing Alzheimer amyloid precursor proteins. Exp Gerontol 1998;33:883–889. [PubMed: 9951631]

Hsiao K, Chapman P, Nilsen S, Eckman C, Harigaya Y, Younkin S, Yang F, Cole G. Correlative memory deficits, Abeta elevation, and amyloid plaques in transgenic mice. Science 1996;274:99–102. [PubMed: 8810256]

Hsieh H, Boehm J, Sato C, Iwatsubo T, Tomita T, Sisodia S, Malinow R. AMPAR removal underlies Abeta-induced synaptic depression and dendritic spine loss. Neuron 2006;52:831–843. [PubMed: 17145504]

Jacobsen JS, Wu CC, Redwine JM, Comery TA, Arias R, Bowlby M, Martone R, Morrison JH, Pangalos MN, Reinhart PH, Bloom FE. Early-onset behavioral and synaptic deficits in a mouse model of Alzheimer's disease. Proc Natl Acad Sci U S A 2006;103:5161–5166. [PubMed: 16549764]

Kamenetz F, Tomita T, Hsieh H, Seabrook G, Borchelt D, Iwatsubo T, Sisodia S, Malinow R. APP processing and synaptic function. Neuron 2003;37:925–937. [PubMed: 12670422]

Kawahara M, Kuroda Y. Molecular mechanism of neurodegeneration induced by Alzheimer's beta-amyloid protein: channel formation and disruption of calcium homeostasis. Brain Res Bull 2000;53:389–397. [PubMed: 11136994]

Kawarabayashi T, Younkin LH, Saido TC, Shoji M, Ashe KH, Younkin SG. Age-dependent changes in brain, CSF, and plasma amyloid (beta) protein in the Tg2576 transgenic mouse model of Alzheimer's disease. J Neurosci 2001;21:372–381. [PubMed: 11160418]

King DL, Arendash GW. Behavioral characterization of the Tg2576 transgenic model of Alzheimer's disease through 19 months. Physiol Behav 2002;75:627–642. [PubMed: 12020728]

Knowles RB, Wyart C, Buldyrev SV, Cruz L, Urbanc B, Hasselmo ME, Stanley HE, Hyman BT. Plaque-induced neurite abnormalities: implications for disruption of neural networks in Alzheimer's disease. Proc Natl Acad Sci U S A 1999;96:5274–5279. [PubMed: 10220456]

Krichmar JL, Nasuto SJ, Scorcioni R, Washington SD, Ascoli GA. Effects of dendritic morphology on CA3 pyramidal cell electrophysiology: a simulation study. Brain Res 2002;941:11–28. [PubMed: 12031543]

Lacor PN, Buniel MC, Chang L, Fernandez SJ, Gong Y, Viola KL, Lambert MP, Velasco PT, Bigio EH, Finch CE, Krafft GA, Klein WL. Synaptic targeting by Alzheimer's-related amyloid beta oligomers. J Neurosci 2004;24:10191–10200. [PubMed: 15537891]

Lacor PN, Buniel MC, Furlow PW, Clemente AS, Velasco PT, Wood M, Viola KL, Klein WL. Abeta oligomer-induced aberrations in synapse composition, shape, and density provide a molecular basis for loss of connectivity in Alzheimer's disease. J Neurosci 2007;27:796–807. [PubMed: 17251419]

Larson J, Lynch G, Games D, Seubert P. Alterations in synaptic transmission and long-term potentiation in hippocampal slices from young and aged PDAPP mice. Brain Res 1999;840:23–35. [PubMed: 10517949]

Lehman EJ, Kulnane LS, Lamb BT. Alterations in beta-amyloid production and deposition in brain regions of two transgenic models. Neurobiol Aging 2003;24:645–653. [PubMed: 12885572]

Lesné S, Koh MT, Kotilinek L, Kayed R, Glabe CG, Yang A, Gallagher M, Ashe KH. A specific amyloid-beta protein assembly in the brain impairs memory. Nature 2006;440:352–357. [PubMed: 16541076]

Luebke JI, Chang YM, Moore TL, Rosene DL. Normal aging results in decreased synaptic excitation and increased synaptic inhibition of layer 2/3 pyramidal cells in the monkey prefrontal cortex. Neuroscience 2004;125:277–288. [PubMed: 15051166]

Luebke JI, Rosene DL. Aging alters dendritic morphology, input resistance, and inhibitory signaling in dentate granule cells of the rhesus monkey. J Comp Neurol 2003;460:573–584. [PubMed: 12717715]

Mainen ZF, Sejnowski TJ. Influence of dendritic structure on firing pattern in model neocortical neurons. Nature 1996;382:363–366. [PubMed: 8684467]

Mattson MP. Calcium and neurodegeneration. Aging Cell 2007;6:337–350. [PubMed: 17328689]

Meyer-Luehmann M, Spires-Jones TL, Prada C, Garcia-Alloza M, de Calignon A, Rozkalne A, Koenigsknecht-Talboo J, Holtzman DM, Bacskai BJ, Hyman BT. Rapid appearance and local

toxicity of amyloid-beta plaques in a mouse model of Alzheimer's disease. Nature 2008;451:720–724. [PubMed: 18256671]

Middei S, Geracitano R, Caprioli A, Mercuri N, Ammassari-Teule M. Preserved fronto-striatal plasticity and enhanced procedural learning in a transgenic mouse model of Alzheimer's disease overexpressing mutant hAPPswe. Learn Mem 2004;11:447–452. [PubMed: 15286183]

Morrison JH, Hof PR. Selective vulnerability of corticocortical and hippocampal circuits in aging and Alzheimer's disease. Prog Brain Res 2002;136:467–486. [PubMed: 12143403]

Nimmrich V, Grimm C, Draguhn A, Barghorn S, Lehmann A, Schoemaker H, Hillen H, Gross G, Ebert U, Bruehl C. Amyloid beta oligomers (A beta(1–42) globulomer) suppress spontaneous synaptic activity by inhibition of P/Q-type calcium currents. J Neurosci 2008;28:788–797. [PubMed: 18216187]

Parameshwaran K, Dhanasekaran M, Suppiramaniam V. Amyloid beta peptides and glutamatergic synaptic dysregulation. Exp Neurol 2008;210:7–13. [PubMed: 18053990]

Qiu WQ, Ferreira A, Miller C, Koo EH, Selkoe DJ. Cell-surface beta-amyloid precursor protein stimulates neurite outgrowth of hippocampal neurons in an isoformdependent manner. J Neurosci 1995;15:2157–2167. [PubMed: 7891158]

Radley JJ, Rocher AB, Rodriguez A, Ehlenberger DB, Dammann M, McEwen BS, Morrison JH, Wearne SL, Hof PR. Repeated stress alters dendritic spine morphology in the rat medial prefrontal cortex. J Comp Neurol 2008;507:1141–1150. [PubMed: 18157834]

Roder S, Danober L, Pozza MF, Lingenhoehl K, Wiederhold KH, Olpe HR. Electrophysiological studies on the hippocampus and prefrontal cortex assessing the effects of amyloidosis in amyloid precursor protein 23 transgenic mice. Neuroscience 2003;120:705–720. [PubMed: 12895511]

Rodriguez A, Ehlenberger D, Kelliher K, Einstein M, Henderson SC, Morrison JH, Hof PR, Wearne SL. Automated reconstruction of three-dimensional neuronal morphology from laser scanning microscopy images. Methods 2003;30:94–105. [PubMed: 12695107]

Rodriguez A, Ehlenberger DB, Hof PR, Wearne SL. Rayburst sampling, an algorithm for automated three-dimensional shape analysis from laser scanning microscopy images. Nat Protoc 2006;1:2152–2161. [PubMed: 17487207]

Romito-DiGiacomo RR, Menegay H, Cicero SA, Herrup K. Effects of Alzheimer's disease on different cortical layers: the role of intrinsic differences in Abeta susceptibility. J Neurosci 2007;27:8496–8504. [PubMed: 17687027]

Saganich MJ, Schroeder BE, Galvan V, Bredesen DE, Koo EH, Heinemann SF. Deficits in synaptic transmission and learning in amyloid precursor protein (APP) transgenic mice require C-terminal cleavage of APP. J Neurosci 2006;26:13428–13436. [PubMed: 17192425]

Shankar GM, Bloodgood BL, Townsend M, Walsh DM, Selkoe DJ, Sabatini BL. Natural oligomers of the Alzheimer amyloid-beta protein induce reversible synapse loss by modulating an NMDA-type glutamate receptor-dependent signaling pathway. J Neurosci 2007;27:2866–2875. [PubMed: 17360908]

Snyder EM, Nong Y, Almeida CG, Paul S, Moran T, Choi EY, Nairn AC, Salter MW, Lombroso PJ, Gouras GK, Greengard P. Regulation of NMDA receptor trafficking by amyloid-beta. Nat Neurosci 2005;8:1051–1058. [PubMed: 16025111]

Spires TL, Hyman BT. Neuronal structure is altered by amyloid plaques. Rev Neurosci 2004;15:267–278. [PubMed: 15526551]

Spires TL, Meyer-Luehmann M, Stern EA, McLean PJ, Skoch J, Nguyen PT, Bacskai BJ, Hyman BT. Dendritic spine abnormalities in amyloid precursor protein transgenic mice demonstrated by gene transfer and intravital multiphoton microscopy. J Neurosci 2005;25:7278–7287. [PubMed: 16079410]

Stern EA, Bacskai BJ, Hickey GA, Attenello FJ, Lombardo JA, Hyman BT. Cortical synaptic integration in vivo is disrupted by amyloid-beta plaques. J Neurosci 2004;24:4535–4540. [PubMed: 15140924]

Takahashi RH, Almeida CG, Kearney PF, Yu F, Lin MT, Milner TA, Gouras GK. Oligomerization of Alzheimer's beta-amyloid within processes and synapses of cultured neurons and brain. J Neurosci 2004;24:3592–3599. [PubMed: 15071107]

Tsai J, Grutzendler J, Duff K, Gan WB. Fibrillar amyloid deposition leads to local synaptic abnormalities and breakage of neuronal branches. Nat Neurosci 2004;7:1181–1183. [PubMed: 15475950]

Urbanc B, Cruz L, Le R, Sanders J, Ashe KH, Duff K, Stanley HE, Irizarry MC, Hyman BT. Neurotoxic effects of thioflavin S-positive amyloid deposits in transgenic mice and Alzheimer's disease. Proc Natl Acad Sci U S A 2002;99:13990–13995. [PubMed: 12374847]

Venkitaramani DV, Chin J, Netzer WJ, Gouras GK, Lesne S, Malinow R, Lombroso PJ. Beta-amyloid modulation of synaptic transmission and plasticity. J Neurosci 2007;27:11832–11837. [PubMed: 17978019]

Vetter P, Roth A, Hausser M. Propagation of action potentials in dendrites depends on dendritic morphology. J Neurophysiol 2001;85:926–937. [PubMed: 11160523]

Walsh DM, Selkoe DJ. Deciphering the molecular basis of memory failure in Alzheimer's disease. Neuron 2004;44:181–193. [PubMed: 15450169]

Wearne SL, Rodriguez A, Ehlenberger DB, Rocher AB, Henderson SC, Hof PR. New techniques for imaging, digitization and analysis of three-dimensional neural morphology on multiple scales. Neuroscience 2005;136:661–680. [PubMed: 16344143]

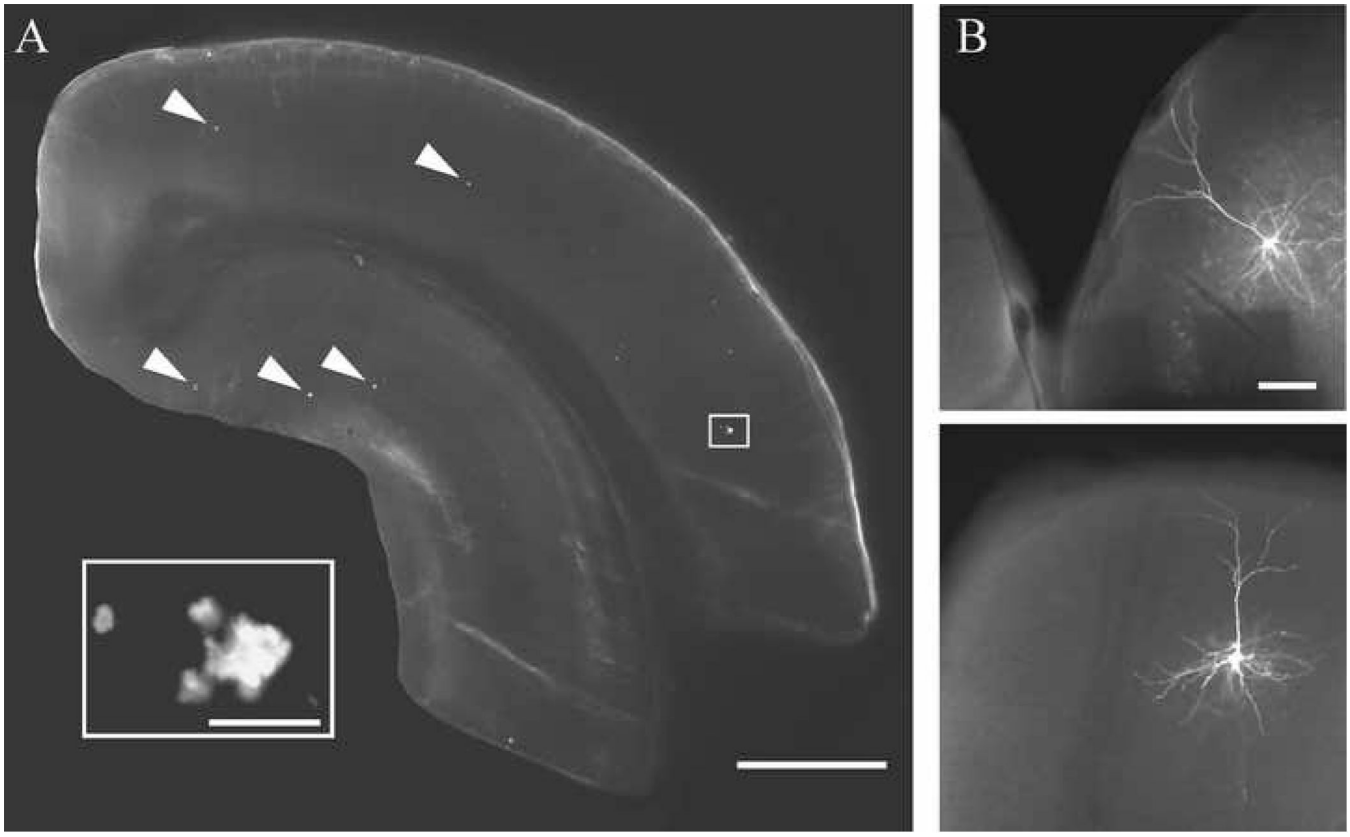

Figure 1. Representative slice and streptavidin-Alexa labeled cells

A. Photomicrograph of a slice from a Tg2576 mouse stained with thioflavin-S showing a low density of fibrillar plaques (arrowheads) in the cortex and hippocampus (inset: boxed area at higher magnification). **B**. Representative streptavidin-Alexa 488 labeled layer 3 pyramidal cells from Tg2576 (top) and Wt (bottom) mice. Scale bars = A: 1 mm, inset: 25 μm; B: 100 μm.

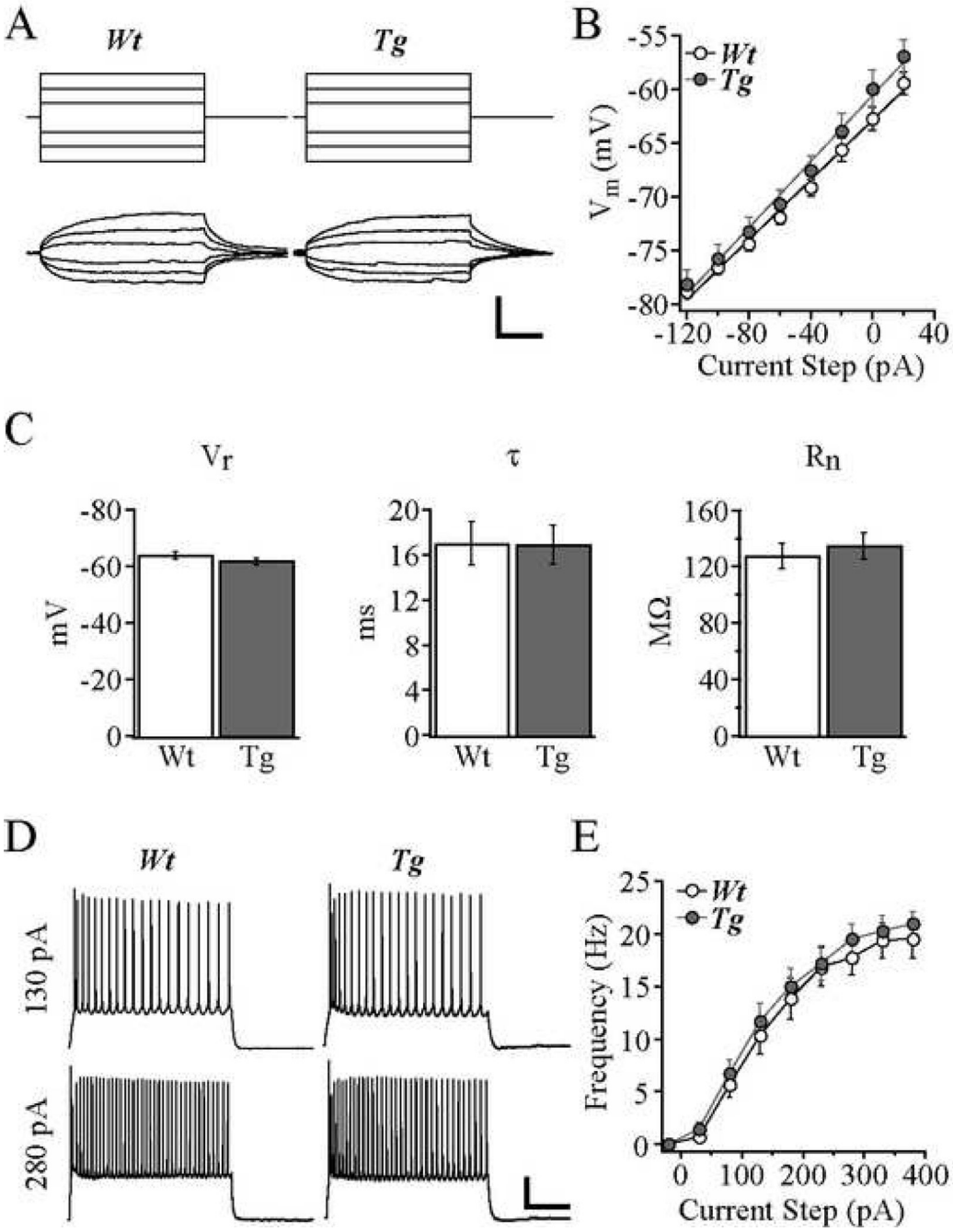

Figure 2. Passive membrane and AP firing properties were unaltered in cells from Tg2576 mice

A. Membrane voltage responses (bottom) to 200 ms injected current steps (top) from representative Wt and Tg2576 cells. **B**. Mean voltage response vs. current step plots for Wt and Tg2576 cells. **C**. Bar graphs demonstrating no significant difference between Wt and Tg2576 cells in terms of mean resting potential, membrane time constant, and input resistance. **D**. Trains of APs evoked by 2s depolarizing current steps of 130 pA (top) and 280 pA (bottom) for Wt and Tg2576 cells. **E**. Frequency-current plot demonstrating unchanged mean frequency of AP firing evoked at each depolarizing current step for Wt and Tg2576 cells. Scale bars = A: 10 mV and 50 ms; D: 20 mV and 500 ms.

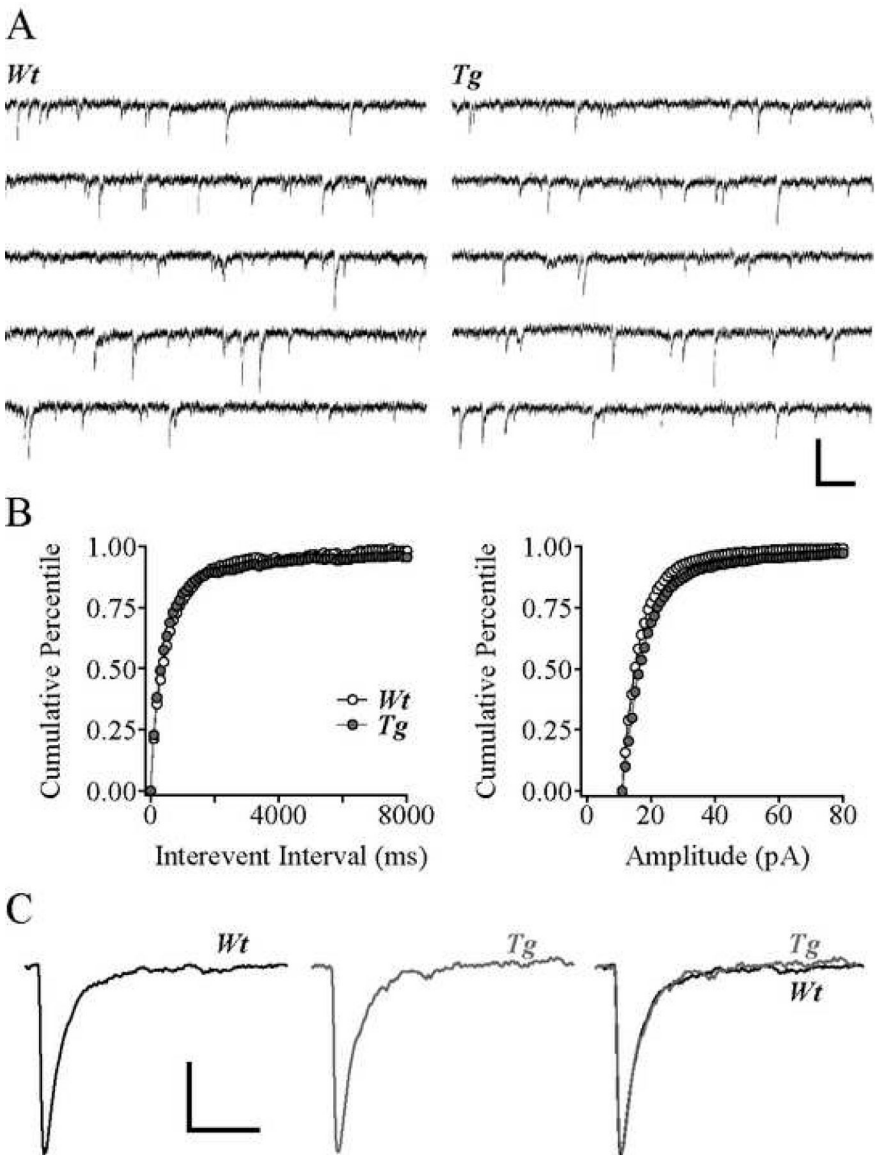

Figure 3. sEPSC properties were unaltered in cells from Tg2576 mice

A. Traces of sEPSCs from representative Wt and Tg2576 cells. **B**. Cumulative percentile plots of inter-event interval (left) and amplitude (right) of sEPSCs in all Wt and Tg2576 cells. **C**. Averaged sEPSCs from representative Wt (left) and Tg2576 (middle) cells, superimposed at right. Scale bars = A: 50 pA and 10 ms; C: 5 pA and 20 ms.

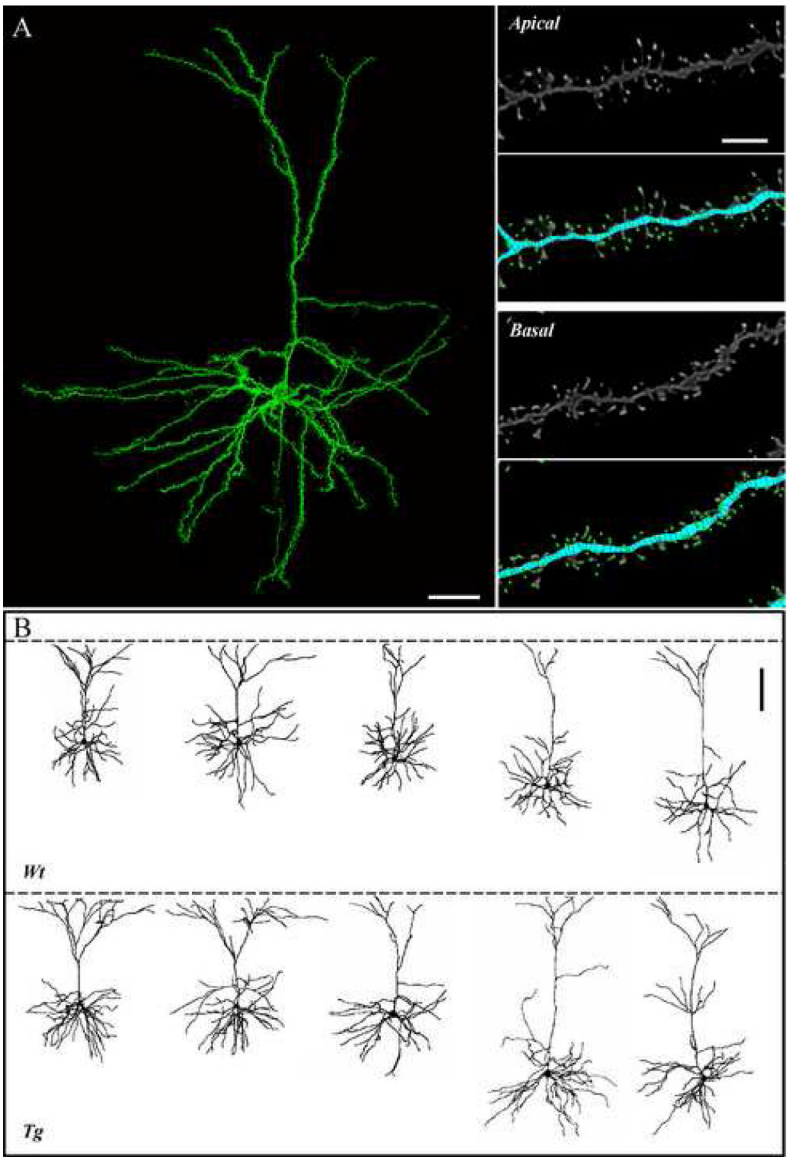

Figure 4. Representative fully reconstructed frontal cortical pyramidal cells of Tg2576 and Wt mice

A. Left: 3D montage of confocal image stacks of a pyramidal cell from a Tg2576 mouse. Right: High magnification view of dendritic segments and spines of the cell in A; raw data are shown in the grey-scale panels; and in the color panels, the same images are shown as digitized by NeuronStudio, with the reconstructed dendrites in blue and the detected spines in green. **B**. Representative reconstructions of Wt (top) and Tg2576 (bottom) cells. Dashed line indicates the pial surface. Scale bars = A: 40 μm; B: 5 μm; C: 100 μm.

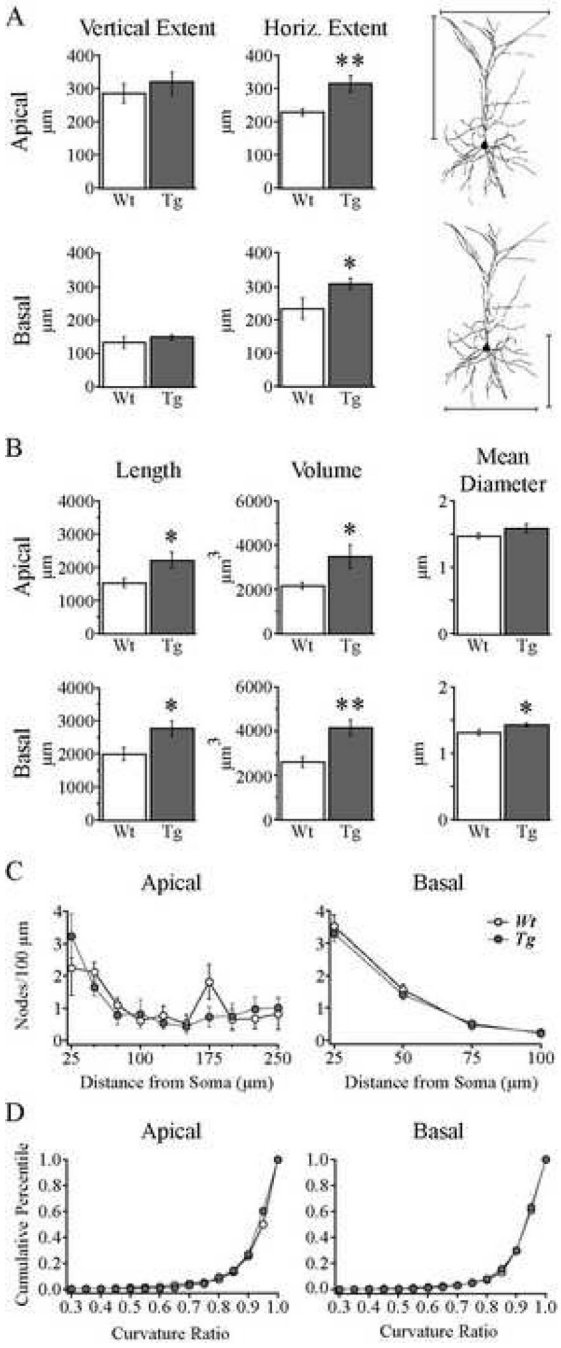

Figure 5. Dendritic length and volume were increased while branching complexity was unaltered in cells from Tg2576 mice

A. Bar graphs demonstrating that the horizontal but not vertical dendritic extents of apical (top) and basal (bottom) dendritic trees were increased in Tg2576 cells. Indication of horizontal and vertical dendritic extents are illustrated to the right. *$p < 0.04$; **$p < 0.01$. **B**. Bar graphs showing significantly increased mean total dendritic volume and length and unaltered mean dendritic diameter for apical (top) and increased mean total dendritic volume, length and dendritic diameter for basal (bottom) dendritic trees. *$p < 0.05$; **$p < 0.002$. **C**. Sholl analysis demonstrating that the number of nodes per 100 µm of dendrite within each 25 µm radial unit distal from the soma were not different in the apical (left) and basal (right) dendritic trees of

Wt vs. Tg2576 cells. **D**. Cumulative percentile plots of the distribution of curvature ratios for all dendritic segments in either apical (left) and basal (right) trees, showing no difference between Wt and Tg2576 cells.

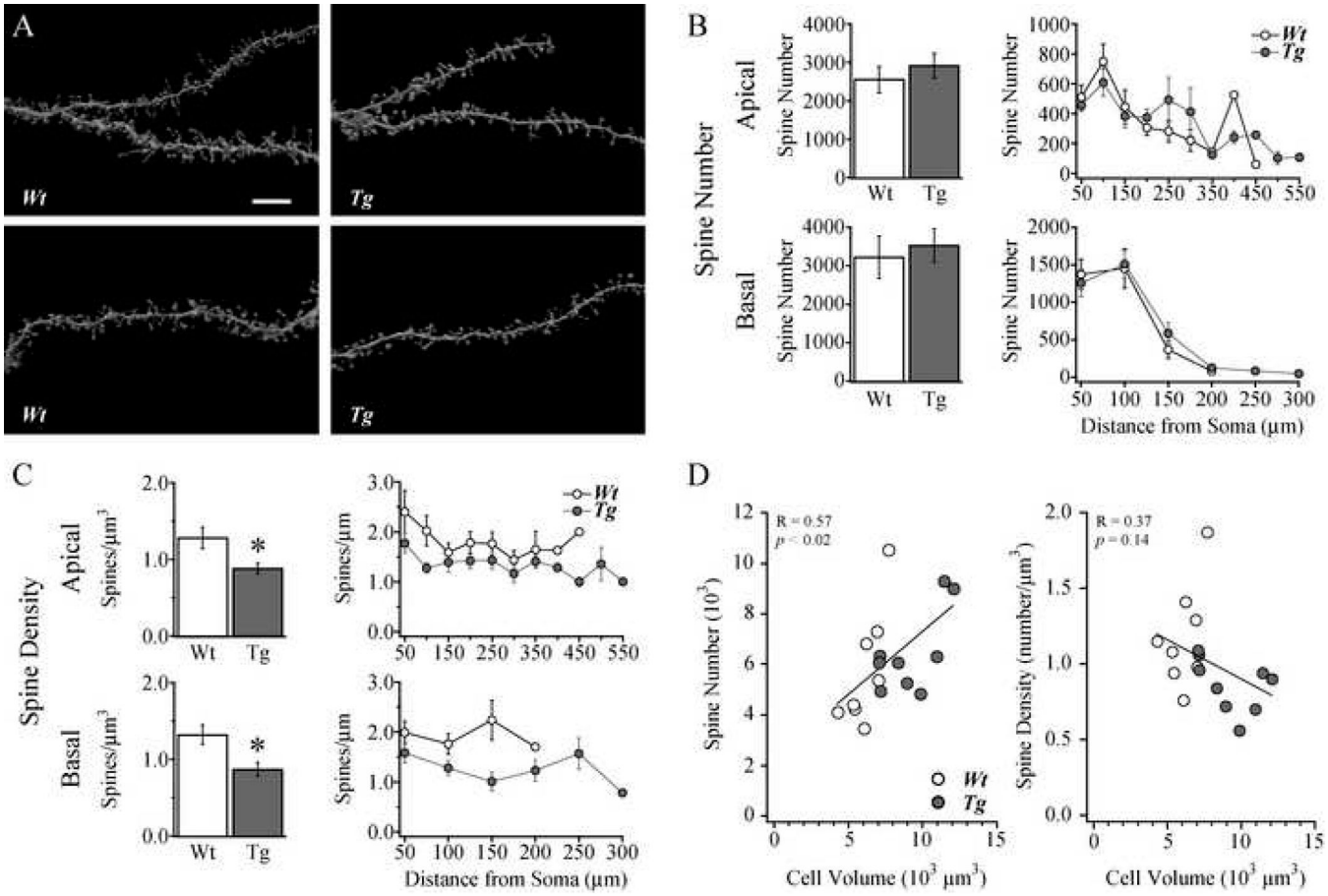

Figure 6. Dendritic spine number was preserved while spine density was decreased in cells from Tg2576 mice

A. Images of apical (top) and basal (bottom) dendritic branch and spine reconstructions from representative Wt (left) Tg2576 (right) cells. **B**. Bar graphs (left) and Sholl analysis (right) demonstrating no significant difference in the total spine numbers in the apical and basal trees in Wt vs. Tg2576 cells. **C**. Bar graphs (left) and Sholl analysis (right) demonstrating a significant decrease in spine density on both apical and basal dendritic trees in Tg2576 cells. * $p < 0.02$. **D**. Scatter plots of spine number (left) and spine density (middle) vs. total cell volume for individual cells, demonstrating a significant relationship with total cell volume for spine number (R = 0.57; $p < 0.02$) but not density (R = 0.38; $p = 0.14$). Scale bar in A = 7 µm.

Table 1

Dendritic and spine characteristics.

Morphological Parameter		**Wt**	**Tg2576**	***p* <**
Vertical dendritic extent (μm)	Apical	285 ± 29	320 ± 36	ns
	Basal	133 ± 17	148 ± 08	ns
Horizontal dendritic extent (μm)	Apical	228 ± 11	314 ± 24	0.01
	Basal	235 ± 31	309 ± 17	0.04
Total dendritic length (μm)	Apical	1529 ± 128	2217 ± 248	0.03
	Basal	1999 ± 200	2778 ± 227	0.02
	Total	3527 ± 209	4995 ± 319	0.002
Total dendritic volume (μm^3)	Apical	2175 ± 149	3502 ± 525	0.03
	Basal	2609 ± 241	4160 ± 351	0.002
	Total	4785 ± 289	7661 ± 654	0.001
Mean dendritic diameter (μm)	Apical	1.47 ± 0.04	1.59 ± 0.07	ns
	Basal	1.31 ± 0.04	1.42 ± 0.03	0.02
	Total	1.40 ± 0.04	1.52 ±0.05	ns
Mean dendritic curvature ratio	Apical	0.91 ± 0.03	0.90 ± 0.02	ns
	Basal	0.91 ± 0.02	0.90 ± 0.01	ns
	Total	0.91 ± 0.02	0.90 ± 0.02	ns
Total number of spines	Apical	2548 ± 343	2919 ± 320	ns
	Basal	3228 ± 553	3533 ± 439	ns
	Total	5775 ± 886	6452 ± 575	ns
Density of spines per μm^3	Apical	1.28 ± 0.14	0.88 ± 0.07	0.02
	Basal	1.32 ± 0.13	0.87 ± 0.09	0.01
	Total	1.19 ± 0.13	0.86 ± 0.06	0.03